Dual Parallel-PMSM System Using Single PMSM Control Hardware: A PLL-Integrated UIO Approach

Tianyi Liu, Zhiming Liu, Fanglai Zhu, and Zhiyang Mao

***Abstract*—A permanent magnet synchronous motor (PMSM) control hardware has integrated two phase-current sensors and a rotor position sensor to realize the control of the motor. Connecting an additional PMSM in parallel without modifying the control hardware would further reduce the cost of building up a multimotor system. However, in this new configuration, not all the necessary information is available directly from the existing sensors, resulting in potential risks in controlling the system properly. In this article, a new unknown input observer (UIO) is developed via interval observer joint phase-lock-loop. The proposed UIO can asymptotically not only estimate the phase current of each motor but also reconstruct the rotor position of the additional motor. Then, a delicately designed controller together with the proposed UIO realizes the speed control of the system. Comprehensive experiments including start-up, speed, and load torque variation verify that the proposed system can achieve the desired goal either in the steady or transient operation state. Moreover, the controller's robustness to variations in stator resistance, inductance, and flux are verified both by simulation and experiment. In this way, without equipping any additional sensors, building a dual parallel PMSM based on conventional single PMSM control hardware is entirely feasible in practice.**

***Index Terms*—Current estimation, interval observer, multipermanent magnet synchronous machine, sensorless, unknown input observer (UIO).**

I. Introduction

With the popularity of permanent magnet synchronous motors (PMSMs) in high-performance driving systems, people always desire a simpler, compacter, and more cost-effective solution. When multiple PMSMs are assigned to the same control objective such as conveyor belts and robotics, the number of controllers and inverters will be increased. Therefore, putting two PMSMs in parallel effectively can reduce the weight and volume of the multimotor driving system, which builds up a monoinverter dual-PMSM system. Its application can vary from low to high power, such as cooling fans [1], conveyor belts [2], and electrical vehicles [3].

In recent years, the control problem of such a dual parallel-PMSM system has been widely studied. The master—slave strategy [4], [5], [6], [7] is widely used, thanks to its stability in highly unbalanced load situations and relatively simple structure. It changes the motor under control in accordance with the load torque. In [5] and [6], the sliding mode controller is used to further improve the dynamic performance of the system. Meanwhile, the necessity to switch the motor under control is also removed. Liu et al. [7] have extended the master-selection criteria so that the motor can work either in motor or brake mode. This method is proven to be able to drive a parallel-PMSM system composed of more than two motors. Liu et al. [8] and Boroujeni and Markadeh [9] have also demonstrated that controlling a dual parallel-PMSM system that involves different motors is also feasible.

A conventional single PMSM controller is usually equipped with two phase-current sensors and a rotor position sensor to control the motor's torque, speed, or position. The existing control hardware is very mature. However, the control strategies mentioned above require current and position feedback of each motor. This means that dedicated control hardware customization is needed including adding current and rotor position sensors for each motor. If we can use a single PMSM control hardware in a dual parallel-connected PMSM (see Fig. 1), the cost of building up a multimotor driving system will be reduced greatly. For example, we can simply put one motor and a controller on one end of the conveyor belt and drive the motor on the other end by only a three-phase line to achieve high-precision synchronization performance.

In this configuration, the current sensor can only measure the total current of each phase, while the rotor position sensor only senses one of the two motors. In this article, we plan to use the observer-based controller to achieve this goal. Under this framework, to realize the control, each motor's phase current ($\hat{I}_{\alpha 1}$, $\hat{I}_{\beta 1}$, $\hat{I}_{\alpha 2}$, $\hat{I}_{\beta 2}$ in Fig. 1) and the rotor position of the second motor ($\hat{\theta}_2$ in Fig. 1) must be reconstructed based on the available sensor information. Sensorless control algorithms for a single PMSM system [10], [11], [12], [13], [14], [15], [16] can only estimate the rotor position when a motor's phase currents are known. Some studies [5], [17] have also focused on the rotor

Manuscript received 7 February 2023; revised 1 July 2023; accepted 22 August 2023. Date of publication 29 August 2023; date of current version 23 October 2023. This research was supported by the National Natural Science Foundation of China under Grants 62203335 and 61973236. Recommended for publication by Associate Editor J. Ye. *(Corresponding author: Fanglai Zhu.)*

Tianyi Liu is with the School of Aerospace Engineering and Applied Mechanics, Tongji University, Shanghai 200092, China (e-mail: tianyi.liu@tongji.edu.cn).

Zhiming Liu and Fanglai Zhu are with the College of Electronics and Information Engineering, Tongji University, Shanghai 200092, China (e-mail: 1933009@tongji.edu.cn; zhufanglai@tongji.edu.cn).

Zhiyang Mao is with the College of Civil Engineering, Tongji University, Shanghai 200092, China (e-mail: 2050240@tongji.edu.cn).

Color versions of one or more figures in this article are available at https://doi.org/10.1109/TPEL.2023.3309901.

Digital Object Identifier 10.1109/TPEL.2023.3309901

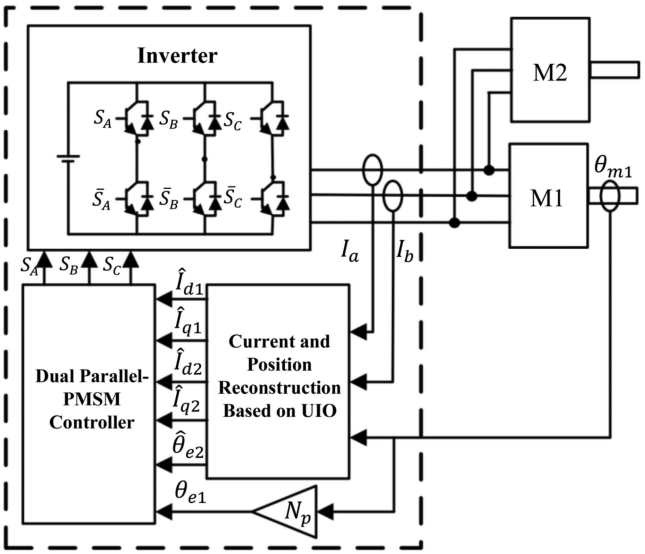

Fig. 1. Proposed system architecture.

position estimation problem of the two motors in a dual parallel-PMSMs system, in which two separate sets of current sensors are still needed, and do not apply to the new system configuration. The simultaneous estimations of the current and position bring a new challenge to the estimation problem of a reduced sensor PMSM system.

To solve the new estimation problem mentioned above, designing an unknown input observer (UIO) which can not only estimate the phase currents of each motor but also reconstruct the rotor position of the additional motor would be one of the best considerations. In view of control theory, the system state estimation and the unknown input reconstruction problem have been investigated intensively for decades. Indeed, for state estimation, a state observer was first constructed by Luenberger in the 1960s [18]. Soon after the Luenberger observer had been proposed, the UIO design issues were raised. During the nascent development such as [19], [20], [21], [22], when designing UIO only for estimating asymptotically the system states, researchers put emphasis mainly on avoiding negative influences caused by the unknown inputs rather than reconstructing them. Since the 1990s, researchers have been interested in simultaneous state and unknown input estimation problems in the field of UIO designs, and many significant results have been reported in literature [23], [24], [25], [26], [27]. For example, Edwards et al. [23] have developed a sliding model observer and adopted the equivalent output injection concept to explicitly reconstruct the fault signal, but this method usually causes chattering effects. In circumstances that the so-called observer matching condition is not satisfied, Kalsi et al. [26] and Zhu [27] deal with the simultaneous state and unknown input estimation problems for linear systems with unknown inputs. However, the output derivative information, which easily causes additional high-frequency noise to the system, is used in reconstructing the unknown input (UI). The UIO design issue is still among the most popular topics in recent years [28], [29], [30], [31], [32], [33], [34], [35].

In the present paper, we introduce a UIO-based control strategy for a dual parallel-PMSM system by developing a novel asymptotic convergence UIO, such that it can be driven by a single PMSM control hardware. The major contributions of the present paper are summarized as follows.

1) An observer design model of the parallel-PMSM system is built in $\alpha\beta$ coordinate and adequately organized. The current and the rotor position are respectively modeled as the system state and the UI of the system. Consequently, the reconstruction problem can be brought into the UIO design domain.
2) Through the constructed model, a novel Luenberger-like state observer together with an unknown input reconstruction is developed via interval observer, which together form a UIO. Moreover, to reconstruct the unknown input, a phase-lock-loop (PLL)-based derivative estimator is also constructed considering the sinusoid signal characteristic of a motor system.
3) By applying the UIO on the parallel-PMSM system, the asymptotic convergence estimations of the phase current of each motor and the rotor position of the additional motor can be obtained, such that driving a dual parallel-PMSM system with a single PMSM control hardware becomes possible. Compared to the existing control schemes, our method leads to a waiver of hardware modification, and the sensorless control problems are further solved.
4) Based on the UIO, we have designed a dedicated controller to implement speed regulation of the system. This controller can operate under highly imbalanced torque. Meanwhile, the controller has strong robustness to parameter variations. Moreover, the system can be normally started without the necessity of knowing all the information of M2 in priori.
5) We have conducted a comprehensive experiment including start-up, speed, and torque variation to validate the feasibility of the proposed system configuration as well as the performance of the UIO-based controller under either steady-state or transient situations. Furthermore, both simulation and experimental analysis are conducted to demonstrate the performance and behavior when parameter variations are presented.

The rest of this article is organized as follows. In Section II, the observer design model of a dual parallel-PMSM system is constructed. In Section III, a novel UIO design method is developed. In Section IV, the description of how to realize the control based on the UIO is provided. In Section V, the simulation and experiment results are illustrated to show the performances of the proposed methods. Finally, Section VI concludes this article.

II. Observer Design Model

In this article, as presented in Fig. 1, we consider two nonsalient pole PMSMs connected in parallel, while only M1 is equipped with a rotor position sensor. Meanwhile, the current sensor can only measure the total current of each phase. The two motors are assumed to be identical. Regarding [10], the

TABLE I
DESCRIPTION OF THE SYMBOL USED IN MODEL

Name	Description
u_α, u_β	Stator voltage in $\alpha\beta$ coordinate
I_α, I_β	Stator current in $\alpha\beta$ coordinate
e_α, e_β	Back electro-motive force in $\alpha\beta$ coordinate
N_p	Number of pole
θ_m	Rotor's mechanical angle
θ_e	Rotor's electrical angle
L_s	Stator windings inductance
φ_f	Permanent magnets flux
R_s	Stator resistance

dual parallel-PMSMs model in the $\alpha\beta$ coordinate is

$$\begin{cases} \frac{dI_{\alpha1}}{dt} = -\frac{1}{L_s}\left(R_sI_{\alpha1} - u_\alpha + e_{\alpha1}\right) \\ \frac{dI_{\beta1}}{dt} = -\frac{1}{L_s}\left(R_sI_{\beta1} - u_\beta + e_{\beta1}\right) \\ \frac{dI_{\alpha2}}{dt} = -\frac{1}{L_s}\left(R_sI_{\alpha2} - u_\alpha + e_{\alpha2}\right) \\ \frac{dI_{\beta2}}{dt} = -\frac{1}{L_s}\left(R_sI_{\beta2} - u_\beta + e_{\beta2}\right). \end{cases} \tag{1}$$

And the measured total current in the $\alpha\beta$ coordinate is

$$\begin{bmatrix} I_\alpha \\ I_\beta \end{bmatrix} = \sqrt{\frac{2}{3}} \begin{bmatrix} 1 & -\frac{1}{2} & -\frac{1}{2} \\ 0 & \frac{\sqrt{3}}{2} & \frac{\sqrt{3}}{2} \end{bmatrix} \begin{bmatrix} I_a \\ I_b \\ -I_a - I_b \end{bmatrix} \tag{2}$$

where I_a and I_b represent the output of the current sensor. Table I illustrates the description of the involved symbols. The parameters and signals of the two motors are identified with the index in the corresponding subscript. It should be noticed that there is no index in u_α and u_β since the two motors are connected in parallel and share the same voltage

$$\begin{aligned} \underbrace{\begin{bmatrix} \frac{dI_{\alpha1}}{dt} \\ \frac{dI_{\beta1}}{dt} \\ \frac{dI_{\alpha2}}{dt} \\ \frac{dI_{\beta2}}{dt} \end{bmatrix}}_{\dot{x}} &= \underbrace{\begin{bmatrix} -\frac{R_s}{L_s} & 0 & 0 & 0 \\ 0 & -\frac{R_s}{L_s} & 0 & 0 \\ 0 & 0 & -\frac{R_s}{L_s} & 0 \\ 0 & 0 & 0 & -\frac{R_s}{L_s} \end{bmatrix}}_{A} \underbrace{\begin{bmatrix} I_{\alpha1} \\ I_{\beta1} \\ I_{\alpha2} \\ I_{\beta2} \end{bmatrix}}_{x} \\ &+ \underbrace{\begin{bmatrix} \frac{1}{L_s} & 0 & -\frac{1}{L_s} & 0 \\ 0 & \frac{1}{L_s} & 0 & -\frac{1}{L_s} \\ \frac{1}{L_s} & 0 & 0 & 0 \\ 0 & \frac{1}{L_s} & 0 & 0 \end{bmatrix}}_{B} \underbrace{\begin{bmatrix} u_\alpha \\ u_\beta \\ e_{\alpha1} \\ e_{\beta1} \end{bmatrix}}_{u} \\ &+ \underbrace{\begin{bmatrix} 0 & 0 \\ 0 & 0 \\ -\frac{1}{L_s} & 0 \\ 0 & -\frac{1}{L_s} \end{bmatrix}}_{D} \underbrace{\begin{bmatrix} e_{\alpha2} \\ e_{\beta2} \end{bmatrix}}_{d} \end{aligned} \tag{3}$$

$$\underbrace{\begin{bmatrix} I_\alpha(t) \\ I_\beta(t) \end{bmatrix}}_{y} = \begin{bmatrix} I_{\alpha1} + I_{\alpha2} \\ I_{\beta1} + I_{\beta2} \end{bmatrix} = \underbrace{\begin{bmatrix} 1 & 0 & 1 & 0 \\ 0 & 1 & 0 & 1 \end{bmatrix}}_{C} x. \tag{4}$$

TABLE II
SYMBOL DESCRIPTION OF THE OBSERVER DESIGN MODEL

Signal Name	Description
x	The internal system state. It describes the phase current of each motor but they are not measurable in our case.
u	The system input. It contains the stator voltage and back EMF of M1 since they are known signal.
d	The system disturbance. It is also the input to the system, but it is unknown. Here it describes the back EMF of M2.
y	The system output. It means the actual measurable signal, which is the total current of the two motors.

But we cannot design a UIO directly on (1). The model needs further processing. The resulting state-space description is given by (3) and (4). In order to adopt it into the upcoming UIO design framework, the back electromotive force (EMF) of M1, that is, $e_{\alpha1}$ and $e_{\beta1}$, together with the input voltage to the motors (u_α and u_β) are treated as input to the system. $e_{\alpha1}$ and $e_{\beta1}$ are expressed by

$$\begin{bmatrix} e_{\alpha1} \\ e_{\beta1} \end{bmatrix} = \begin{bmatrix} \sin\theta_{e1} \\ \cos\theta_{e1} \end{bmatrix} \omega_{e1}\varphi_f$$

since M1 is equipped with a rotor position sensor. ω_{e1} is the rotor's electrical speed of M1. They are known to be the observer. On the other hand, the back EMF of M2 is modeled as an unknown input to the system, which is indicated as d in (3). It will be reconstructed by the proposed UIO. And consequently, the M2's electrical position can be calculated by the following:

$$\hat{\theta}_{e2} = -\tan^{-1}\frac{\hat{e}_{\alpha2}}{\hat{e}_{\beta2}}. \tag{5}$$

Moreover, the system state x describes the phase current of each motor expressed in alpha–beta coordinate and y implies the actual current sensor architecture. Table II gives a more comprehensive description of the state variable. Finally, we can describe the model in a more compact form as follows:

$$\begin{cases} \dot{x} = Ax + Bu + Dd \\ y = Cx \end{cases}. \tag{6}$$

A UIO will be constructed based on the model (3), (4) to asymptotically estimate x and reconstruct the UI d simultaneously only by using the information of u and y.

III. UNKNOWN INPUT OBSERVER DESIGN

To construct a UIO with the function of providing the asymptotic convergence estimations of x and d simultaneously, denoted as $\hat{x}$ and $\hat{d}$ respectively, in this section, we have used an interval observer (IO) to set up an algebraic relationship between the unknown input d and the system state x in advance. Then, based on this relationship, the desired UIO design method is developed.

A. Preliminaries

Before proceeding to the observer design, some preliminaries should be given first.

Notation 1: For any matrix $\Lambda \in R^{n\times m}$, we define $\Lambda^+ = \max(0,\Lambda)$, $\Lambda^- = \max(0,-\Lambda)$. $|\Lambda|$ is a $n\times m$ matrix whose corresponding elements are the absolute value of matrix Λ. Obviously, we have $\Lambda = \Lambda^+ - \Lambda^-$ and $|\Lambda| = \Lambda^+ + \Lambda^-$.

Notation 2: diag(w) stands for a diagonal matrix with the elements of w being as its diagonal elements.

Notation 3: If two matrices or vectors, *A* and *B*, have the same dimensions, $A \le B$ is compared elementwise.

Precondition 1: The unknown input d has constant upper and lower boundaries such that $\underline{d} \le d \le \bar{d}$, where $\underline{d}$ and $\bar{d}$ are two known constant vectors. The initial state $x(0)$ is unknown but bounded with $\underline{x}_0 \le x(0) \le \bar{x}_0$, and $\underline{x}_0$ and $\bar{x}_0$ are two constant known vectors.

This precondition is general due to the physical limitation of the back-EMF and current of the PMSM, which are represented as d and x, respectively.

Precondition 2: The rank condition rank $\begin{bmatrix} sI_n - A & D \\ C & 0 \end{bmatrix} = n+q$ holds for any complex s with Re$(s) \ge 0$. n and q are the order of x and d, respectively.

Precondition 3: The rank condition rank $(CD) =$ rank $(D) = q$ holds

$$\begin{cases} \dot{\breve{x}} = (A-MC)\,\bar{x} + Bu + My + D^+\bar{d} - D^-\underline{d} \\ \dot{\underline{x}} = (A-MC)\,\underline{x} + Bu + My + D^+\underline{d} - D^-\bar{d} \end{cases} \tag{7}$$

$$\begin{cases} \dot{\hat{x}} = A\hat{x} + Bu + D\hat{d} + L\,(y - C\hat{x}) \\ \hat{d} = (CD)^\dagger \left[\text{diag}\left(f_1\left(\breve{x}\right)\right)\alpha + \text{diag}\left(\breve{y}\right)\hat{\alpha} + f_2\left(\underline{x}, y\right) \right. \\ \qquad \left. - CA\hat{x}\right] \end{cases} \tag{8}$$

with

$$f_1\left(\breve{x}\right) = C\,(A-MC)\breve{x} + C\,|D|\breve{d} \tag{9}$$

$$f_2\left(\underline{x}, y\right) = C\left[(A-MC)\,\underline{x} + My + D^+\underline{d} - D^-\bar{d}\right]. \tag{10}$$

Under *Precondition* 3, we know that the pseudo inverse of CD, which is $(CD)^\dagger = \left[(CD)^T(CD)\right]^{-1}(CD)^T$, exists.

Lemma 1: Under *Precondition* 2, the pair

$$\left(\left(I_n - D(CD)^\dagger C\right)A, C\right)$$

is detectable.

Proof: Under *Precondition 2*, we have

$$\begin{aligned} n+q &= \text{rank}\begin{bmatrix} sI_n - A & D \\ C & 0 \end{bmatrix} \\ &= \text{rank}\left\{\begin{bmatrix} sI_n - A & D \\ C & 0 \end{bmatrix}\begin{bmatrix} I_n & 0 \\ (CD)^\dagger CA & I_q \end{bmatrix}\right\} \\ &= \text{rank}\begin{bmatrix} sI_n - A + D(CD)^\dagger CA & D \\ C & 0 \end{bmatrix} \end{aligned}$$

holds for any complex s with $Re(s) \ge 0$, which implies that

$$\text{rank}\begin{bmatrix} sI_n - \left(I_n - D(CD)^\dagger C\right)A \\ C \end{bmatrix} = n$$

holds for any complex s with Re$(s) \ge 0$. And consequently, the pair $((I_n - D(CD)^\dagger C)A, C)$ is detectable by definition [36].

B. TIO Design

In the first step, we design an IO that is expressed in (7) for system (6). From (7), we can easily deduce that

$$\dot{\breve{x}} = (A - MC)\ \breve{x} + |D|\ \breve{d}, \tag{11}$$

where $\breve{x} = \bar{x} - \underline{x}$ and $\breve{d} = \bar{d} - \underline{d}$.

Lemma 2: [37]*:* (7) is an interval observer of the system (6) in which $\underline{x}(t) \le x(t) \le \bar{x}(t)$ holds for all $t \ge 0$ if the initial states are set as $\bar{x}\,(0) = \bar{x}_0$ and $\underline{x}(0) = \underline{x}_0$ and the gain matrix *M* is selected such that $A - MC$ is not only Hurwitz but also Metzler.

Notice that $C \ge 0$, the interval estimation of the original system output *y* can also be described by the following:

$$\begin{cases} \underline{y} = C\underline{x} \\ \bar{y} = C\bar{x} \end{cases} \tag{12}$$

such that $\underline{y} < y < \bar{y}$ holds. Moreover, we have

$$\breve{y} = \bar{y} - \underline{y} = C\breve{x}. \tag{13}$$

C. UIO Design

Denote $y = [y_1 \quad y_2]^T$, $\bar{y} = [\bar{y}_1 \quad \bar{y}_2]^T$ and $\underline{y} = [\underline{y}_1 \quad \underline{y}_2]^T$. Since $\underline{y} \le y \le \bar{y}$ implies that $\underline{y}_i \le y_i \le \bar{y}_i$, $(i = 1,2)$, it can be concluded that there exist time-varying scalars $\alpha_i(t)$ satisfying $0 \le \alpha_i(t) \le 1$ such that

$$y_i = \alpha_i\left(\bar{y}_i - \underline{y}_i\right) + \underline{y}_i,\ (i = 1,2).$$

The time scaler *t* will be omitted if no confusion arises. They can also be written compactly as follows:

$$y = \text{diag}\left(\breve{y}\right)\alpha + \underline{y} \tag{14}$$

with $\alpha = \begin{bmatrix}\alpha_1 & \alpha_2\end{bmatrix}^T$. Make a derivative of (13) and use (11), we have

$$\dot{\breve{y}} = C\ \dot{\breve{x}} = f_1\ \left(\breve{x}\right) \tag{15}$$

where $f_1(\breve{x})$ is described in (9). Moreover, there is

$$\dot{\underline{y}} = f_2\ (\underline{x}, y) + CBu \tag{16}$$

where $f_2(\underline{x}, y)$ is described in (10). Now making a derivative on (14) and substituting the corresponding elements with (15) and (16), it gives

$$\dot{y} = \text{diag}\left(f_1\left(\breve{x}\right)\right)\alpha + \text{diag}\left(\breve{y}\right)\dot{\alpha} + f_2\left(\underline{x}, y\right) + CBu. \tag{17}$$

On the other hand, it follows from (6) that

$$\dot{y} = C\,\dot{x} = CAx + CBu + CDd. \tag{18}$$

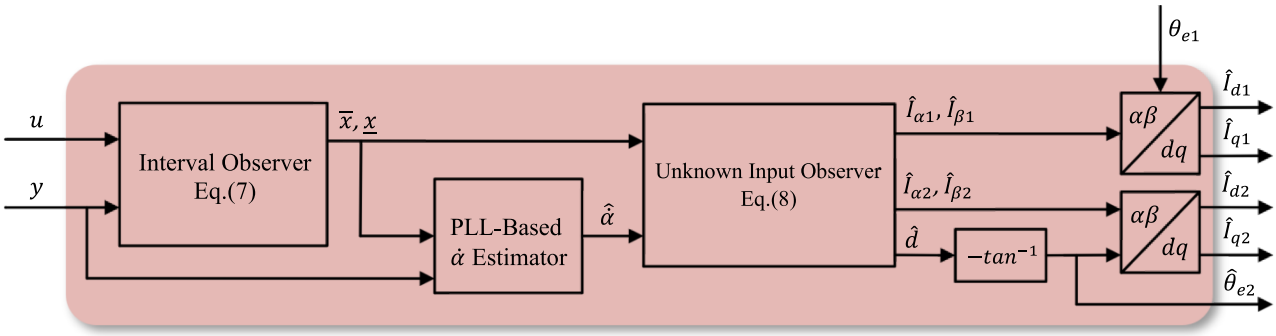

Fig. 2. Overall structure of the UIO.

Therefore, by comparing (17) and (18) we have

$$CDd = \operatorname{diag}\left(f_1\left(\breve{x}\right)\right)\alpha + \operatorname{diag}\left(\breve{y}\right)\dot{\alpha} + f_2\left(\underline{x}, y\right) - CAx. \tag{19}$$

Under *Precondition 3*, from (19) we can obtain

$$d = (CD)^{\dagger}\left[\operatorname{diag}\left(f_1\left(\breve{x}\right)\right)\alpha + \operatorname{diag}\left(\breve{y}\right)\dot{\alpha} + f_2\left(\underline{x}, y\right) - CAx\right] \tag{20}$$

which is an algebraic relationship between the unknown input d and the system state x. Moreover, it follows from (14) that

$$\alpha = \left(\operatorname{diag}\left(\breve{y} + \gamma\right)\right)^{-1}\left(y - \underline{y}\right) \tag{21}$$

where $\gamma = \begin{bmatrix}\gamma_1 & \gamma_2\end{bmatrix}^T$, and $\gamma_i = 1$ if $\overline{y}_i = \underline{y}_i$; otherwise, $\gamma_i = 0$ $(i = 12)$. Now, the desired UIO is constructed by (8) by referring to (20). Then, we have the main result as follows:

Theorem 1: Under *Preconditions 1–3*, system (8) is a UIO of the system (6) which can asymptotically produce both the state estimation $\hat{x}$ and the unknown input $\hat{d}$, satisfying $\lim_{t\to\infty}\tilde{x}(t) = 0$ and $\lim_{t\to\infty}\tilde{d}(t) = 0$, where $\tilde{x}(t) = x(t) - \hat{x}(t)$ and $\tilde{d}(t) = d(t) - \hat{d}(t)$. Here α is determined by (21), and $\widehat{\dot{\alpha}}$ is the identical estimate of $\dot{\alpha}$ which will be provided by a PLL based estimator. It is introduced in the next part.

Proof: By subtracting the first equation of (8) from (6), we can obtain the observer error dynamic as

$$\dot{\tilde{x}} = (A - LC)\,\tilde{x} + D\tilde{d}. \tag{22}$$

Similarly, subtracting the second equation of (8) from (20) leads to

$$\tilde{d} = (CD)^{\dagger}\ \operatorname{diag}\left(\hat{y}\right)\widetilde{\dot{\alpha}} - (CD)^{\dagger}\,CA\tilde{x} \tag{23}$$

where $\widetilde{\dot{\alpha}} = \dot{\alpha} - \widehat{\dot{\alpha}}$. Moreover, substituting (23) into (22) yields

$$\dot{\tilde{x}} = \left(A - D(CD)^{\dagger}CA - LC\right)\tilde{x} + D(CD)^{\dagger}\operatorname{diag}\left(\breve{y}\right)\widetilde{\dot{\alpha}}. \tag{24}$$

We assume $\widetilde{\dot{\alpha}} = 0$ due to the fact that the estimation of $\dot{\alpha}$ is identical. Therefore, (24) turns out to be

$$\dot{\tilde{x}} = \left(A - D(CD)^{\dagger}CA - LC\right)\tilde{x}. \tag{25}$$

Now, based on Lemma 1, we must specify the observer gain matrix L such that (25) convergent asymptotically. Thus, we have

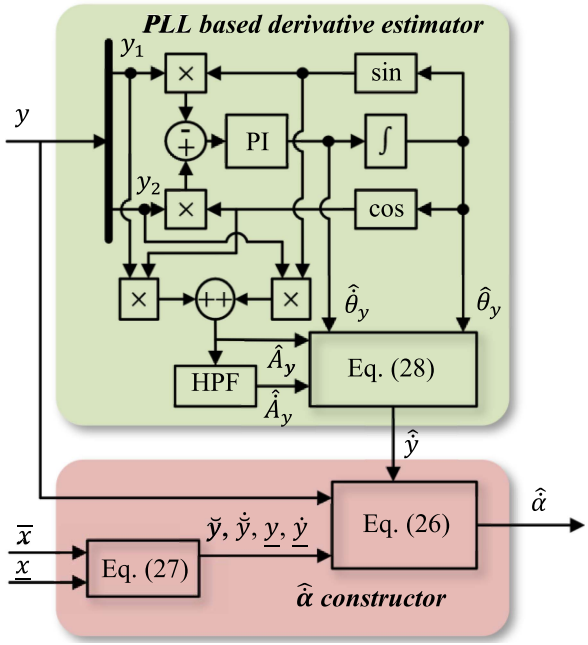

Fig. 3. Proposed PLL-based $\dot{\boldsymbol{\alpha}}$ estimator.

$\lim_{t\to\infty}\tilde{x}(t) = 0$. Meanwhile, $\lim_{t\to\infty}\tilde{d}(t) = 0$ is also achieved as indicated in (23). This ends the proof of Theorem 1.

Remark 1: A UIO is given by (7)–(10). The proposed unknown input reconstruction determined by the second equation of (8) has two significant features. First, it provides an asymptotical estimation of the actual unknown input, which is essential to the proposed system. Second, the unknown input reconstruction decouples the control input u and this will reduce the difficulty in designing a controller. Fig. 2 illustrates the overall structure of the UIO.

D. PLL-Based Estimator of $\dot{\alpha}$

The proposed UIO needs an estimation of the first-order derivative of α. Various estimators, such as super-twisting algorithm [38], can achieve this goal. But in this article, a PLL based estimator is constructed considering the sinusoid characteristic of α as well as avoid chattering problems in the estimation result.

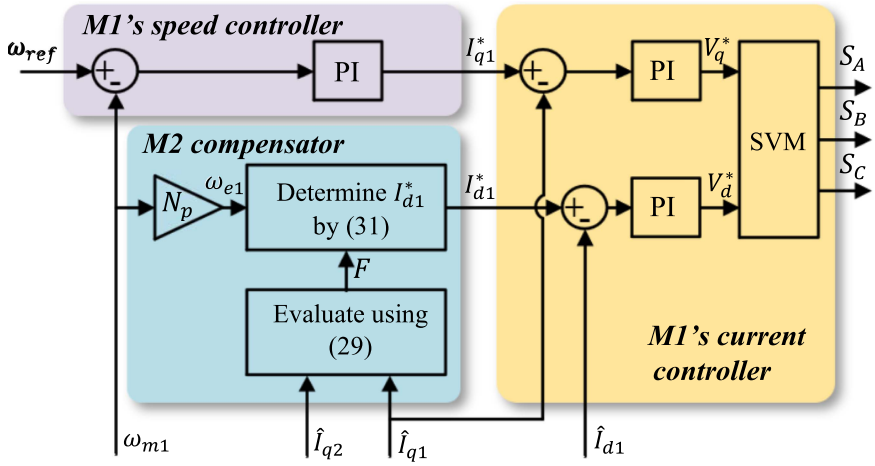

Fig. 4. Block diagram of the non-master-selection control strategy.

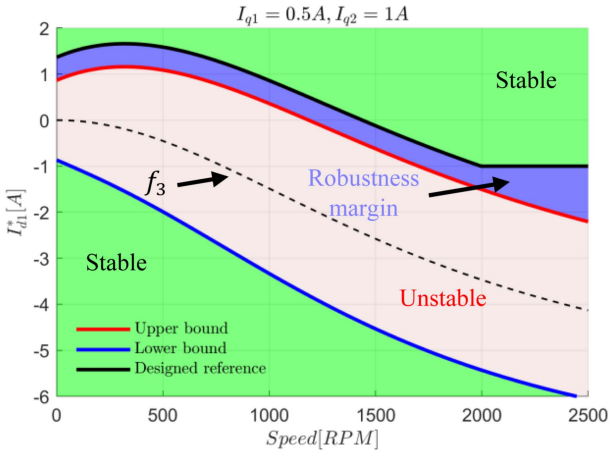

Fig. 5. Designed robustness margin when $I_{q1} = 0.5$ A and $I_{q2} = 1$ A.

Making a derivative on (21), we can obtain

$$\dot{\alpha} = \begin{bmatrix} -\frac{1}{\breve{y}_1^2}\dot{\breve{y}}_1\left(y_1 - \underset{\sim}{y}_1\right) + \frac{1}{\breve{y}_1}\left(\dot{y}_1 - \dot{\underset{\sim}{y}}_1\right) \\ -\frac{1}{\breve{y}_2^2}\dot{\breve{y}}_2\left(y_2 - \underset{\sim}{y}_2\right) + \frac{1}{\breve{y}_2}\left(\dot{y}_2 - \dot{\underset{\sim}{y}}_2\right) \end{bmatrix} \tag{26}$$

where $\breve{y} = \begin{bmatrix} \breve{y}_1 & \breve{y}_2 \end{bmatrix}^T$, $\dot{\breve{y}} = \begin{bmatrix} \dot{\breve{y}}_1 & \dot{\breve{y}}_2 \end{bmatrix}^T$, $\underset{\sim}{y} = \begin{bmatrix} \underset{\sim}{y}_1 & \underset{\sim}{y}_2 \end{bmatrix}^T$, $\dot{\underset{\sim}{y}} = \begin{bmatrix} \dot{\underset{\sim}{y}}_1 & \dot{\underset{\sim}{y}}_2 \end{bmatrix}^T$. Among them, $\breve{y}, \dot{\breve{y}}, \underset{\sim}{y}, \dot{\underset{\sim}{y}}$, and y are known concerning (12), (13), (15), (16). For better representation, we summarize again these equations here as follows:

$$\begin{cases} \breve{y} = C\breve{x} \\ \dot{\breve{y}} = C\left(A - MC\right)\breve{x} + C\left|D\right|\breve{d} \\ \underset{\sim}{y} = C\underset{\sim}{x} \\ \dot{\underset{\sim}{y}} = f_2\left(\underset{\sim}{x}, y\right) + CBu. \end{cases} \tag{27}$$

Thus, it is only necessary to estimate $\dot{y}$ to construct $\widehat{\dot{\alpha}}$. Considering that y is the total phase current of the two parallel-connected motors in $\alpha\beta$ coordinate, without losing generality, we can assume

$$y\ (t) = A_y\ (t)\begin{bmatrix} \cos\left(\theta_y\left(t\right)\right) \\ \sin\left(\theta_y\left(t\right)\right) \end{bmatrix}$$

where $A_y(t)$ is the amplitude and $\theta_y(t)$ is the phase of the current vector. And consequently, its derivative is

$$\dot{y} = \dot{A}_y \begin{bmatrix} \cos\left(\theta_y\right) \\ \sin\left(\theta_y\right) \end{bmatrix} + A_y\dot{\theta}_y \begin{bmatrix} -\sin\left(\theta_y\right) \\ \cos\left(\theta_y\right) \end{bmatrix}. \tag{28}$$

To estimate $\dot{y}$, that is $\widehat{\dot{y}}$, we need to estimate: A_y, $\dot{A}_y$, θ_y, and $\dot{\theta}_y$, which are represented as $\hat{A}_y$, $\widehat{\dot{A}}_y$, $\hat{\theta}_y$, $\widehat{\dot{\theta}}_y$ respectively. Therefore, a PLL [39] can achieve this goal. A traditional PLL can output $\hat{\theta}_y$, and $\widehat{\dot{\theta}}_y$ so that we upgrade it to make it output also $\hat{A}_y$ and $\widehat{\dot{A}}_y$. The complete diagram of the proposed estimator is shown in Fig. 3. For $\hat{A}_y$, we use $\cos(\hat{\theta}_y)$ and $\sin(\hat{\theta}_y)$ multiply y_1 and y_2 respectively. Then, a high-pass filter is used to estimate $\dot{A}_y$. Eventually, $\dot{\alpha}$ can be estimated together with (26) and (28) by replacing the signal with estimated ones.

IV. Controller Design

To realize the control, in this article, we have chosen the non-master-selection control scheme proposed in [7]. It proves to be able to work under highly unbalanced load situations as well as has the advantages that there is no need to switch the motor under control and it doesn't rely on the speed information of M2. It involves a compensator that regulates I_{d1} to keep global stability, thanks to the open-loop stability characteristic.

A. Definition of the Control Scheme

The control scheme proposed in [7] whose working principle is illustrated by Fig. 4 also supports more than two motors connected in parallel to operate but considering that in our case there are only two motors, the corresponding priority evaluation becomes

$$F = \left[\hat{I}_{q2}\left(\hat{I}_{q2} + 2T_e^n\right) - \hat{I}_{q1}\left(\hat{I}_{q1} + 2T_e^n\right)\right] \tag{29}$$

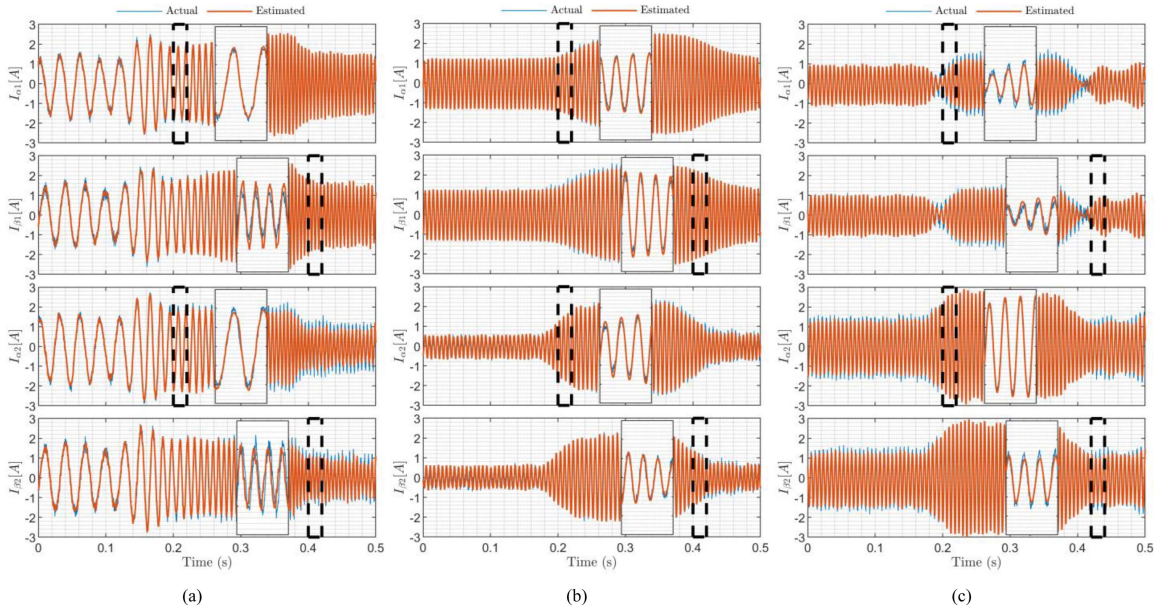

Fig. 6. Comparison of the estimated and actual current in $\alpha\beta$ coordinate. (a) Speed variation. (b) Load applied to M1. (c) Load applied to M2.

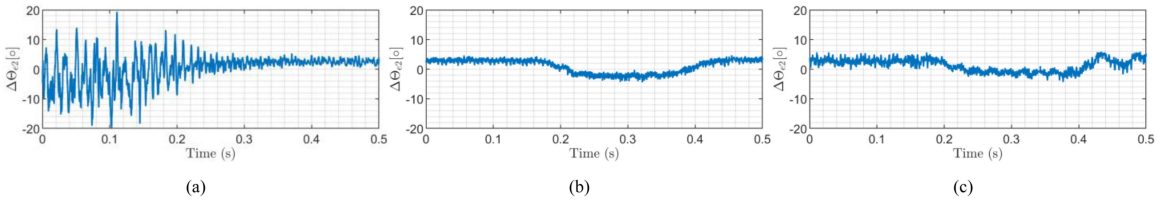

Fig. 7. Estimation error of $\hat{\boldsymbol{\theta}}_{e2}$. (a) Speed variation. (b) Load applied to M1. (c) Load applied to M2.

where $T_e^n = \frac{R_s \omega_{e1} \varphi_f}{R_s^2 + (L_s \omega_{e1})^2}$.

It should be noticed that this controller needs two identical motors, which implies $R_s = R_{s1} = R_{s2}$ and $L_s = L_{s1} = L_{s2}$. Then, depending on the value of (29), the reference of I_{d1} is bounded by

$$\begin{cases} (-\infty,\ f_3 - \sqrt{F}\,] \cup [\,f_3 + \sqrt{F}\ , +\infty) & F > 0 \\ (-\infty, +\infty) & F \le 0 \end{cases} \tag{30}$$

with $f_3 = -\frac{L_s \omega_{e1}^2 \varphi_f}{R_s^2 + (L_s \omega_{e1})^2}$. When $F \le 0$, M1 is "more loaded" than M2, the system is stable even I_{d1} is arbitrary. Otherwise, M2 is "more loaded" and I_{d1} must be regulated inside the region specified by (30) to ensure the system's stability. The quotation means the load can be positive or negative, either means in motor mode or generator mode.

B. Robustness and Start-Up Consideration

Equation (30) has only given the stable boundary of the system, depending on the motor we used in the experiment, we have specified the I_{d1}^* to be

$$\begin{cases} \max\left(f_3 + \sqrt{F} + 0.5, -1\right) & F > 0 \\ \max\left(f_3 + 0.5, -1\right) & F \le 0 \end{cases} \tag{31}$$

which applies an additional margin (0.5 A) to the stable boundary. Meanwhile, I_{d1}^* is given a minimal value at –1 A. Fig. 5 illustrates to speed when M2 is more loaded ($I_{q1} = 0.5$ A, $I_{q1} = 1$ A). M2 is stable only when I_{d1}^* is in the green area which is defined by (30). Our considerations are as follows.

1) Make the current not overrated when speed varies: Due to the contribution of f_3, it equals 0 when the motors stop and goes to minus as speed increases. Thus, such specification can limit I_{d1}^* from -1 to 0.5 unless highly unbalanced torques are applied.
2) Increase the system's robustness: The stable boundary (30) defines the I_{d1} which corresponds to a minimum voltage required to make M2 stable. Thus, a margin applied to it also increases this voltage and consequently the robustness.
3) To properly start the system: When the system starts, its speed at that point is close to zero, which means that the stable boundary is also almost zero due to f_3. Thus, without the necessity to know the information of M2, the system is always stable as long as $I_{d1} > 0$ is imposed. Since M1 is equipped with an encoder, it is not difficult to achieve this goal.

V. Simulation and Experiment

In this section, the performance and characteristics of the proposed UIO are evaluated with either simulation or experiment. The two motors used are identical. The simulation mainly concerns the influence of parameter variation of each motor

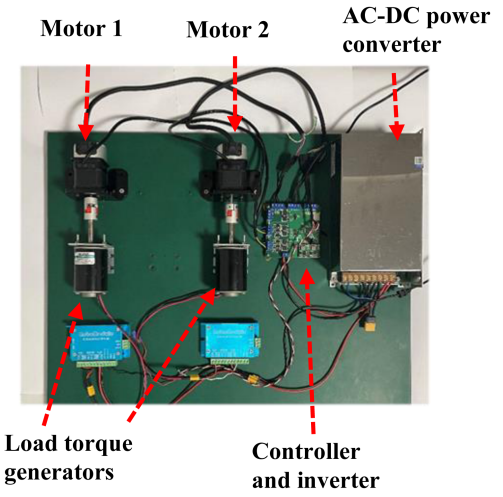

Fig. 8. Experiment bench.

TABLE III
PARAMETERS OF THE EXPERIMENT MOTORS

	Description	Value	Unit
R_s	Stator phase resistance	1.2	Ω
L_s	Stator phase inductance	1.625	mH
φ_f	Amplitude of the flux due to the magnets	9×10^{-3}	V/rad
N_p	Number of pairs of poles	4	
V_{dc}	DC bus Voltage	24	V
P_n	Nominal power	32	W
ω_n	Nominal speed	2500	r/min
I_n	Nominal current	1.4	A

the observer are changed by ±25% from their nominal value to see the possible influence on the observer output.

While in the experiments, all motors are put under different operation situations including start-up, speed variation, and external load transition, to evaluate the feasibility of the proposed system configuration as well as the performance of the reconstruction algorithm. In the experiment, all motors are equipped with dedicated sensors in order to better demonstrate the observer performance by comparing the estimated value with the actual ones from the sensors.

Fig. 8 demonstrates the experimental bench. The parameters of the experimental motors are shown in Table III. Two identical PMSMs, together with two dc motors that served as controllable torque-generators, which are driven by two commercial dc motor controllers, are involved in the experiment. The torque reference can be deduced from the pulsewidth modulation (PWM) signal gained from the PMSM controller. The experimental machine integrates an encoder with a resolution of 1000 pulses per mechanical round, meaning giving a resolution of the electrical angle equals $360° \times 4 \div 1000 = 1.44°$. The sensor sampling, control command loop, and reconstruction algorithm run at 10 kHz.

Considering that there are many independent estimation values to be recorded at 10 kHz, rather than let the microcontroller output them to an oscilloscope, we have integrated a SD card on the control board so that all measured and estimated data from the controller can be stored inside it and analyzed on the computer.

A. Parameter of the Observer Gain Matrix

The UIO has two matrices to be designed: M and L so as to make (11) and (25), which are the dynamic of the interval observer and current observation error, stable with adequate performance.

In this article, we design *M* as

$$M = \begin{bmatrix} m_1 & 0 & m_2 & 0 \\ 0 & m_1 & 0 & m_2 \end{bmatrix}^T.$$

The eigenvalues of $A - MC$ consequently are

$$-\frac{R_s}{L_s}, -\frac{R_s}{L_s}, -\frac{R_s}{L_s} - m_1 - m_2, -\frac{R_s}{L_s} - m_1 + m_2.$$

This implies that the interval observer has two invariant poles at $-\frac{R_s}{L_s}$. Obviously, for a motor, these two poles are stable since R_{s1} and L_{s1} are always larger than zero. While two other poles can be tuned by properly setting the value of m_1 and m_2, to make the observer stable, $A - MC$ is Metzler, and adjust the performance of it. In the experiment, we have set $m_1 = 100$, $m_2 = 200$ to put the poles at –750, –750, –1050, –650.

Meanwhile, *L* can be designed as

$$\begin{bmatrix} l_1 & 0 & l_2 & 0 \\ 0 & l_1 & 0 & l_2 \end{bmatrix}^T$$

so that the eigenvalues of $A - D(CD)^{\dagger}CA - LC$ are $-\frac{R_s}{L_s}, -\frac{R_s}{L_s}, -l_1 - l_2, -l_1 - l_2$.

It also has two invariant poles at $-\frac{R_s}{L_s}$. In the experiment, we have set $l_1 = 200$, $l_2 = 300$ to allocate the eigenvalues at –750, –750, –500, –500.

B. Discretization of the Observer

The observer must be discrete considering that it has to run inside a microcontroller. In this article, we have used forward Euler to achieve this goal. The dynamic systems, including (7) and (8), after discretization are shown in (32). T_s corresponds to the sampling frequency of the observer, which is 100 μs in our case. We have used $u(k-1)$ rather than $u(k)$ since the measured sensor information is the result excited by the voltage applied in the last PWM period

$$\begin{aligned} \bar{x}(k+1) &= (I + T_s(A - MC))\bar{x}(k) \\ &\quad + T_s\left[Bu(k-1) + My(k) + D^{+}\bar{d} - D^{-}\underline{d}\right] \\ \underline{x}(k+1) &= (I + T_s(A - MC))\underline{x}(k) \\ &\quad + T_s\left[Bu(k-1) + My(k) + D^{+}\underline{d} - D^{-}\bar{d}\right] \\ \hat{x}(k+1) &= (I + T_s(A - LC))\hat{x}(k) \end{aligned}$$

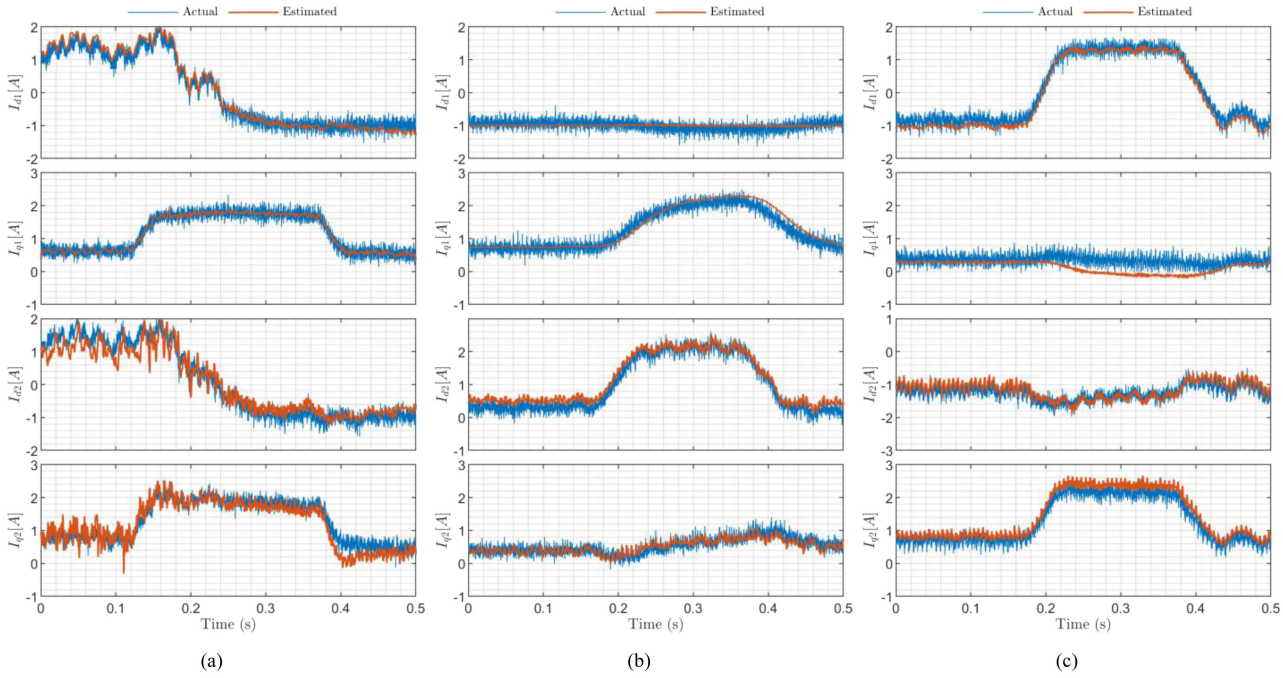

Fig. 9. Comparison of the estimated and actual current in d–q coordinate of (a) speed variation; (b) load applied to M1; (c) load applied to M2.

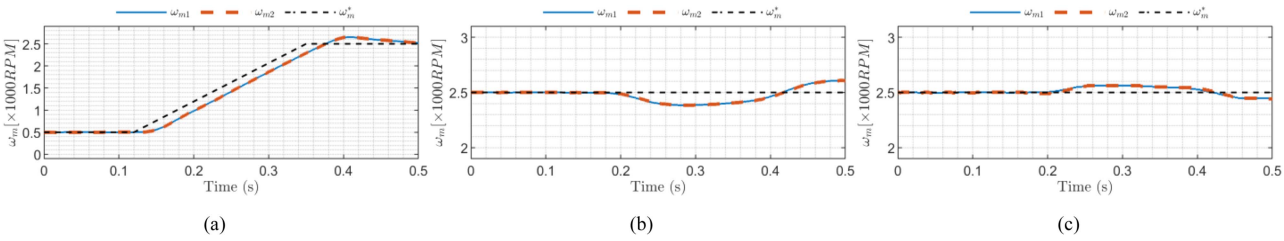

Fig. 10. Speed response of (a) speed variation; (b) load applied to M1; (c) load applied to M2.

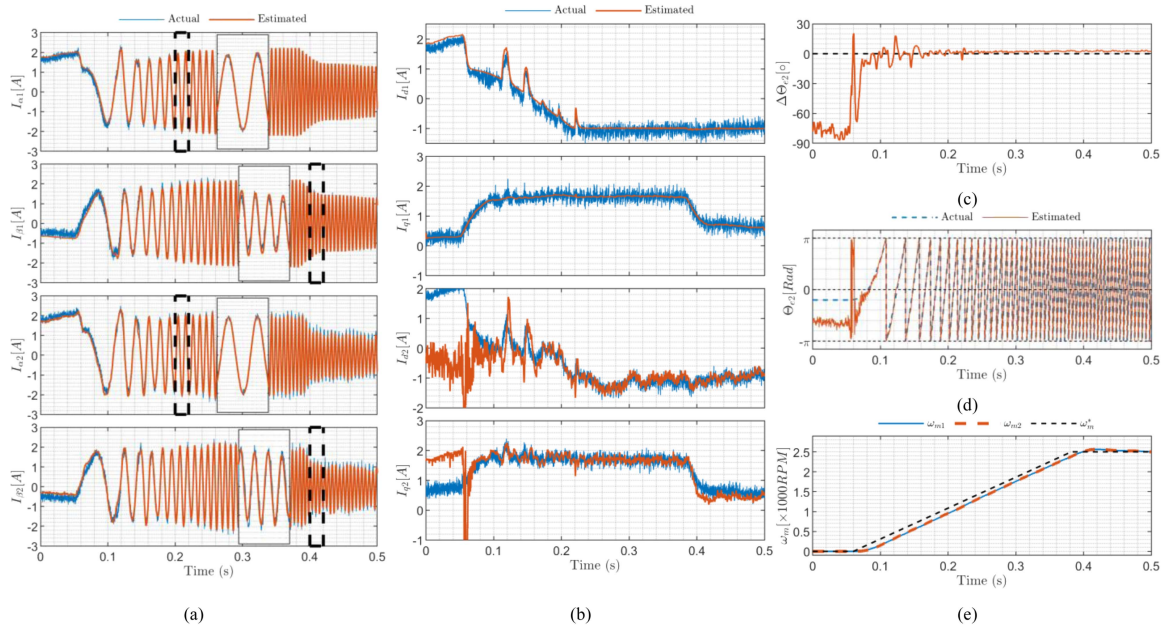

Fig. 11. Start-up experiment results. (a) Actual and estimated current in $\boldsymbol{\alpha\beta}$ coordinate. (b) Actual and estimated current in dq coordinate. (c) Estimation error of $\hat{\boldsymbol{\theta}}_{\mathbf{e}2}$; (d) $\boldsymbol{\theta}_{\mathbf{e}2}$ and $\hat{\boldsymbol{\theta}}_{\mathbf{e}2}$. (e) Mechanical speed ($\boldsymbol{\omega_m}$) response.

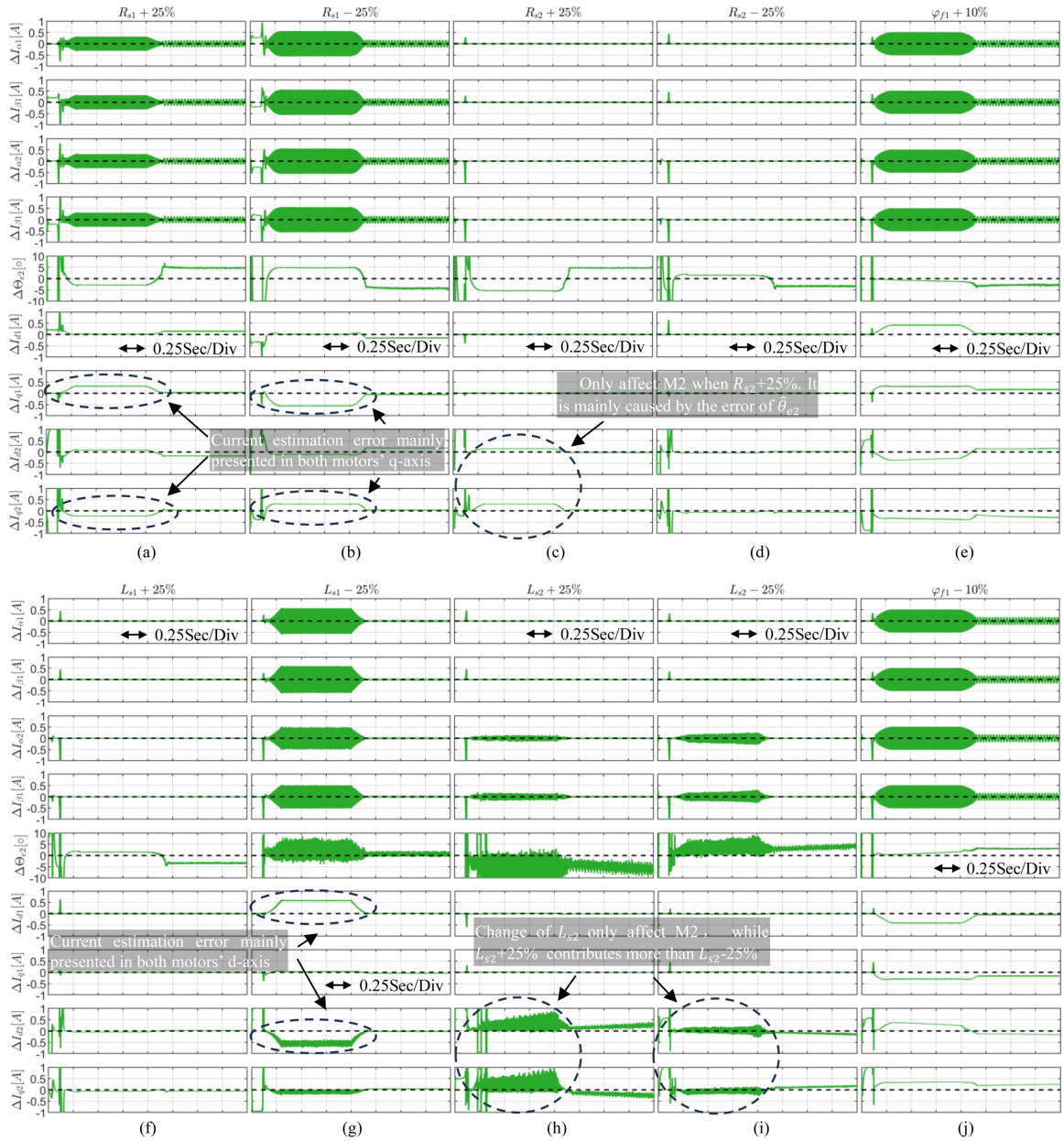

Fig. 12. Results of the parameter variation simulation. (a) R_{s1}+25%. (b) R_{s1}–25%. (c) R_{s2}+25%. (d) R_{s2}–25%. (e) φ_{f1} +10%. (f) L_{s1}+25%. (g) L_{s1}–25%. (h) L_{s2}+25%. (i) L_{s2}–25%. (j) φ_{f1} –10%.

$$+ T_s \left[Bu\left(k-1\right) + D\hat{d}\left(k\right) + Ly\left(k\right) \right]. \quad (32)$$

C. Speed Variation Experiment

This experiment is conducted in order to test the UIO performance when the machines' speed is either high or low. In the experiment, two motors are first operating at 500 r/min. Then, the speed command is raised to 2500 r/min. Meanwhile, the torque generators apply static load torque to both motors.

Fig. 6(a) shows the actual and estimated current of both motors in the $\alpha\beta$ coordinate. It shows that when the speed is changing, the estimated current can also keep tracking (see the enlarged figure).

Fig. 7(a) shows the estimation error of $\hat{\theta}_2$, it is calculated by

$$\Delta\,\hat{\theta}_{e2} = \sin^{-1}\left(\sin\left(\theta_{e2} - \hat{\theta}_{e2}\right)\right) \quad (33)$$

for a better illustration. $\hat{\theta}_{e2}$ is calculated by (5). $\hat{\theta}_{e2}$ has more ripples in the low-speed region than that in the high-speed region. The corresponding currents in the *dq* coordinate [see Fig. 9(a)] also indicate the influence. A static error around 2.5°can also be observed, but it causes a minor influence on the response.

The response of I_{d1} in Fig. 10(a) shows that the control strategy is compensating for the speed variation to make the system stable. As specified by (31), it decreases as the speed increase and is limited to –1 A. But it raises at 0.15 and 0.22 s due to the increase of M2's torque.

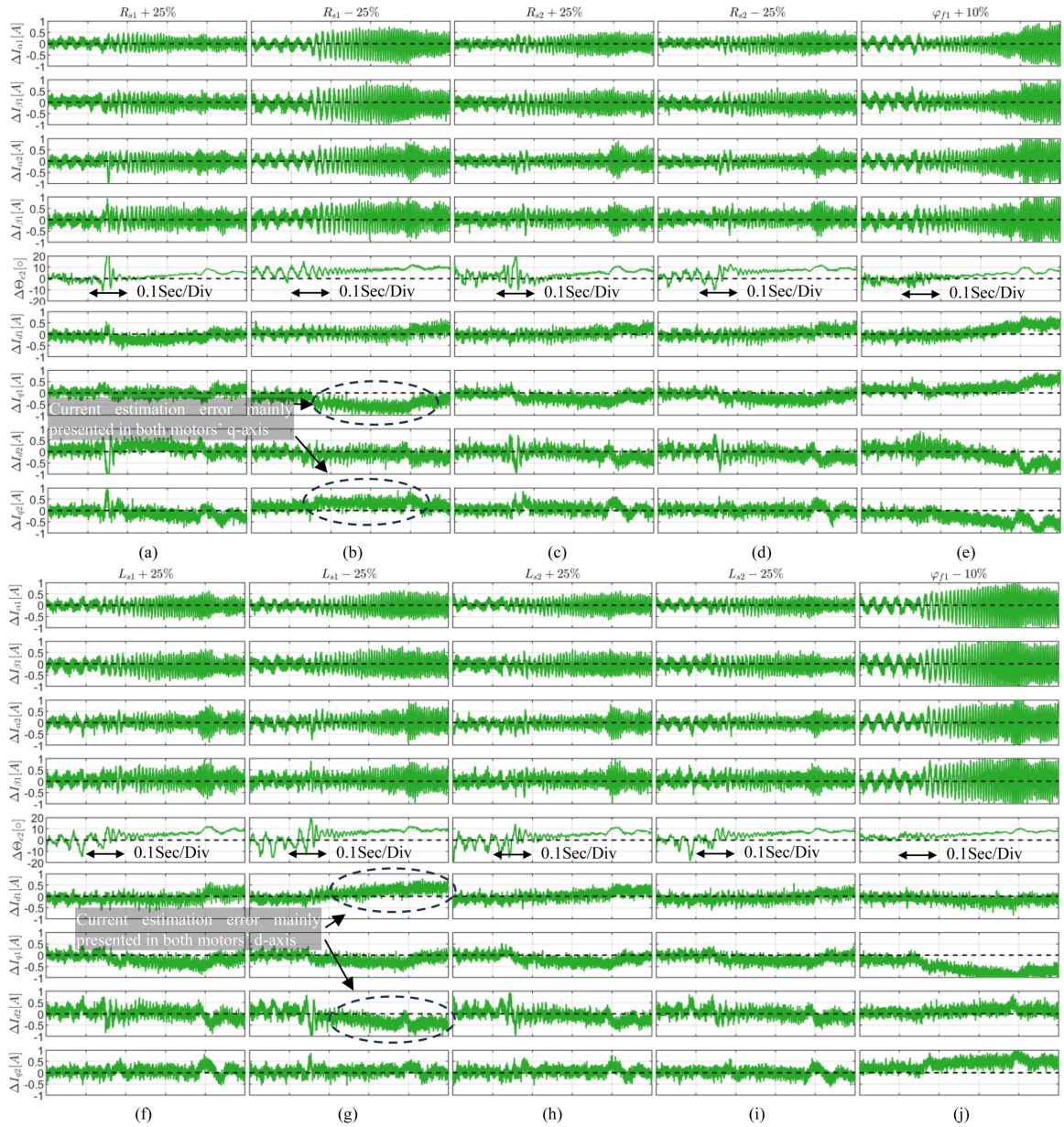

Fig. 13. Results of the parameter variation experiment. (a) R_{s1}+25%. (b) R_{s1}–25%. (c) R_{s2}+25%. (d) R_{s2}–25%. (e) φ_{f1} +10%. (f) L_{s1}+25%. (g) L_{s1}–25%. (h) L_{s2}+25%. (i) L_{s2}–25%. (j) φ_{f1} –10%.

Fig. 10(a) indicates the speed response. Even if some observation error is present, the control strategy can still make the system stable and track the given speed reference.

D. Load Variation Experiment

This experiment is used to verify the performance of the control strategy together with the UIO when an external load is applied to either M1 or M2. During the experiment, each motor is applied with a load more than four times higher than the other one. Meanwhile, the phase current is two times higher than the nominal current. With these efforts, the system stability under extremely imbalanced situations can be verified.

Figs. 7(b)–10(b) show the corresponding result of M1, while Figs. 7(c)–10(c) are for M2. The proposed control strategy can work well under all conditions. In Fig. 6(b) when M1 is applied load (at around 0.18 s), both motors' currents are increased. From Fig. 9(b) we can see that the current increment of M1 is on the q-axis to compensate for the load. $\hat{I}_{d1}$ is constantly regulated at –1 A since M1 is always the more loaded motor but slight variation in the actual value are presented. On the other hand, the current increment of M2 is on the d-axis. This is because the controller must increase the voltage to compensate for the increment of the torque on M1, while for M2, the increased voltage also leads to an increment in its current since the two motors are in parallel. As M2's torque is not changed, its current increment could only happen on the d-axis.

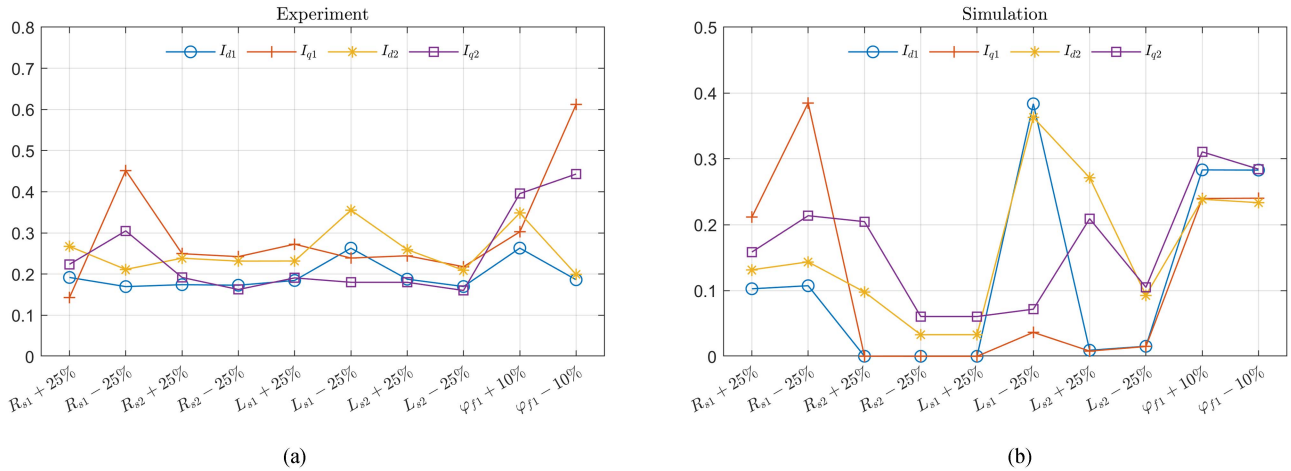

Fig. 14. RMS value of the current estimation error in *dq* coordinate of the (a) simulation and (b) experiment.

Fig. 7(b) also shows that $\hat{\theta}_{e2}$ are affected on this occasion with variation from 2.5°to –2.5°. The speed response [see Fig. 10(b)] shows that the system is stable and both motors have good synchronous condition.

When M2 is applied with an external load, the results are almost the same. The major difference is that at 0.18 s, $\hat{I}_{d1}$ is significantly increased to compensate for the torque increase of M2 so as to guarantee system stability.

E. Start-Up Experiment

Fig. 11 demonstrates the start-up experiment results. In order to better describe the start-up mechanism, we discuss the two motors separately. For the M1, which is the closed-loop controlled one, the system must be first excited by applying a small voltage (2 V in our case). This excitation procedure is common since PMSM equipped with a relative position encoder needs to be aligned before starting. During the alignment, the UIO can also output the correct estimation of current [illustrated in Fig. 11(a)]. This is because there is $d = 0$ (back EMF of M2 is zero) when both motors stop and $\hat{x}$ must be close to the actual value. Considering that the control strategy only controls M1 while M2 is in open-loop, since M1 is equipped with a position sensor, the controller has full information about M1 and can start it normally.

On the other hand, the start-up of M2 can be divided into two situations. The first case is when M1 is more loaded. The system can normally start without the necessity to know the information of M2 since in this situation, the system is always stable (defined by (30) when $F \leq 0$). The second case is that M2 is more loaded. In this case, the I_{d1} corresponding to the stable boundary is zero since the speed is zero [calculated by (30)]. Since we have added a 0.5 A margin to this boundary, M2 is always stable independent of its current and correctness of the angle position. After start-up, the proposed UIO also converges fast enough to make the proper operation of M2. From Fig. 11(c) and (d) we can conclude that, just after both motors start, it takes only 20 ms for the UIO to output the correct $\hat{\theta}_{e2}$ even though the speed is very low. After 0.08 s from the beginning of the experiment, the UIO can output the correct $\hat{\theta}_{e2}$ as well as the current [shown in Fig. 11(b)].

The above results have verified that the proposed control strategy combined with the UIO can successfully reconstruct the current of both two motors and the rotor position of M2 simultaneously in either steady or transient operation state. Although some estimation errors are present, especially in transient situations, and may be caused by the parameter variation during the experiment, these errors are at the same level as a conventional PMSM sensorless [12], [13], [14], [15] and the controller can still handle them to make the system operate normally.

F. Parameter Variation Tests

We have undertaken both simulation and experiment in order to evaluate the performance of the system when parameter uncertainty is presented, whose results are presented in Figs. 12 and 13. The corresponding variables of these figures are indicated as Δ since they illustrate the observation error rather than the actual result to have a better representation of the influence. To better evaluate the influence in view of the controller, the estimation error in the *dq* coordinate is also given. During the simulation, the two motors start up at 0.25 s and then reach 2500 r/min to evaluate the stability. At 1 s, a speed change is applied to bring them back to 500 r/min to see the influence caused by speed variation. While for the experiment, the same condition in speed variation test is applied. For each motor, its R_s and L_s are changed by $\pm 25\%$, and φ_{f1} for $\pm 10\%$ in sequence in every simulation or experiment run. To clarify more, here the $+25\%$ means the corresponding parameter used in the observer is 25% higher than the actual one.

Fig. 12(a)–(d) are the results when the stator resistance of each motor is changed $\pm 25\%$ from its nominal value. We can see an interesting phenomenon that changes in R_{s2} can hardly influence $\hat{x}$, while R_{s1}–25% may cause more error than in the case of $R_{s1} + 25\%$, especially in the high-speed region. The corresponding errors in the *dq* coordinate indicate that the estimation errors when R_{s1} changing are mainly in *q*-axis.

In steady state, the error is constant so that integrators in the controller can generally compensate for it. The speed response also confirms this conclusion.

Meanwhile, the simulation results of inductance variation are shown in Fig. 12(f)–(i). It can be concluded that compared to stator resistance, the observation error is more likely affected by speed since both $\hat{x}$ and $\hat{\theta}_{e2}$ present more ripple in the high-speed region than in the low-speed. Especially, L_{s1}–25% cause more significant errors than others. The response in the *dq* coordinate also gives the same conclusion. But compared to the results when R_{s1} variates, the errors mainly occur in the *d*-axis. Thus, an accurate estimation of inductance, especially for M1, may be needed to minimize the observation error.

Fig. 12(e) and (j) illustrate the simulation results then the flux change. Compared to other parameters, even it is only changed by 10%, the variation of flux causes relatively significate errors in both *d*-axis and *q*-axis of the two motors. Its influence must be carefully considered.

Fig. 13 shows the experiment results. Due to the sensor noise and other error sources, the influence of parameter uncertainty is not as clear as it is in the simulation. But we can still judge some obvious differences in Fig. 13(b) and (g). In Fig. 13(b), current estimation errors are mainly presented in *q*-axis when R_{s1} is changed by –25%. On the contrary, estimation errors occur in *d*-axis when L_{s1} is changed by –25%, which is consistent with the conclusion in the simulation.

To better compare the simulation and experiment results, in Fig. 14 we have presented the root mean squared (RMS) value of the current estimation error in the *dq* coordinate for both the simulation and the experiment. We can find that their results meet well qualitative. When concerning changes in R_s and L_s, R_{s1}–25% and L_{s1}–25% cause more influence than other variations in them. Thus, in practice, by simply setting a higher value than the nominal one can relieve the impact of the variation of R_s and L_s. Moreover, their influence has a directional characteristic that mainly exists on either *q*-axis or *d*-axis, respectively. Meanwhile, changes in flux cause significant influence in all the estimated values even if it is only changed by 10%.

In conclusion, parameter mismatch does cause performance degradation to the UIO. Among them, the accuracy of the parameters of M1 plays a major role while those of M2 cause minor errors. However, the controller can compensate for the errors to ensure the system's stability remains and well track the speed reference, even in the worst case.

VI. Conclusion

In this article, a new observer-based control strategy is proposed for the dual parallel-PMSM built with single PMSM control hardware. Due to the reduced sensor in the new architecture, an IO-based UIO is constructed to estimate the rotor position and the current information for both motors simultaneously. Then the non-master-selection strategy is used to realize the system speed-tracking operation through estimated information.

The experimental results of start-up, speed, and load variation show that the proposed system architecture is fully feasible in practice. It is also indicated that some estimation errors are still presented in the result, especially when motors are not in steady-state. Then, both the simulation and the experiment demonstrate the possible influence caused by stator resistance, inductance, and flux variation. The results indicate that the parameters of M1, especially for R_{s1}–25% and L_{s1}–25%, cause a more significant influence on the estimation error than that of M2. A "configuration-free" might be possible to let people connect M2 without the necessity to configure the controller from the point of view of the observer.

In the next step, we will further improve the performance of the observer by analytically studying the parameter influence in the orientation of obtaining a clear relationship between the error and the parameter so that proper methods can be used to optimize the performance.

References

[1] X. Xu, G. Zhou, J. Rao, and G. Yang, "Study and design of low-speed direct-driven permanent magnet synchronous machines(PMSM) for fan used on power air cooling island," in *Proc. 20th Int. Conf. Elect. Mach. Syst.*, 2017, pp. 1–5.

[2] X. Nian and Z. Deng, "Robust synchronization controller design of a two coupling permanent magnet synchronous motors system," *Trans. Inst. Meas. Control*, vol. 37, no. 8, pp. 1026–1038, Sep. 2015.

[3] M. Al Sakka et al., "Comparative analysis of single-input multi-output inverter topologies for multi-motor drive systems," in *Proc. 15th Int. Conf. Ecological Veh. Renewable Energies*, 2020, pp. 1–12.

[4] D. Bidart, M. Pietrzak-David, P. Maussion, and M. Fadel, "Mono inverter multi-parallel permanent magnet synchronous motor: Structure and control strategy," *IET Elect. Power Appl.*, vol. 5, no. 3, pp. 288–294, Mar. 2011.

[5] T.-I. Yeam and D.-C. Lee, "Design of sliding-mode speed controller with active damping control for single-inverter dual-PMSM drive systems," *IEEE Trans. Power Electron.*, vol. 36, no. 5, pp. 5794–5801, May 2021.

[6] J. Lee and J.-W. Choi, "MTPA control method for MIDP SPMSM drive system using angle difference controller and P&O algorithm," *IEEE Trans. Power Electron.*, vol. 37, no. 12, pp. 15382–15396, Dec. 2022.

[7] T. Liu, M. Fadel, J. Li, and X. Ma, "A MTPA control strategy for mono-inverter multi-PMSM system," *IEEE Trans. Power Electron.*, vol. 36, no. 6, pp. 7165–7177, Jun. 2021.

[8] T. Liu, Z. Liu, and F. Zhu, "A nonlinear robust speed controller for dual nonidentical parallel PMSM system," *IEEE Trans. Power Electron.*, vol. 37, no. 9, pp. 10190–10199, Sep. 2022.

[9] M. M. Boroujeni and G. A. Markadeh, "Energy-based control technique for monoinverter dual parallel PMSM with different parameters," *IEEE Trans. Ind. Electron.*, vol. 69, no. 12, pp. 12162–12172, Dec. 2022.

[10] D. Liang, J. Li, R. Qu, and W. Kong, "Adaptive second-order sliding-mode observer for PMSM sensorless control considering VSI nonlinearity," *IEEE Trans. Power Electron.*, vol. 33, no. 10, pp. 8994–9004, Oct. 2018.

[11] Z. Novak and M. Novak, "Adaptive PLL-based sensorless control for improved dynamics of high-speed PMSM," *IEEE Trans. Power Electron.*, vol. 37, no. 9, pp. 10154–10165, Sep. 2022.

[12] W. Zhu, S. Li, H. Du, and X. Yu, "Nonsmooth observer-based sensorless speed control for permanent magnet synchronous motor," *IEEE Trans. Ind. Electron.*, vol. 69, no. 12, pp. 13514–13523, Dec. 2022.

[13] Q. Tang, A. Shen, X. Luo, and J. Xu, "PMSM sensorless control by injecting HF pulsating carrier signal into ABC frame," *IEEE Trans. Power Electron.*, vol. 32, no. 5, pp. 3767–3776, May 2017.

[14] W. Xu, Y. Jiang, C. Mu, and F. Blaabjerg, "Improved nonlinear flux observer-based second-order SOIFO for PMSM sensorless control," *IEEE Trans. Power Electron.*, vol. 34, no. 1, pp. 565–579, Jan. 2019.

[15] Y. Shao, Y. Yu, F. Chai, and T. Chen, "A two-degree-of-freedom structure-based backstepping observer for DC error suppression in sensorless PMSM drives," *IEEE Trans. Ind. Electron.*, vol. 69, no. 11, pp. 10846–10858, Nov. 2022.

[16] G. Wang, M. Valla, and J. Solsona, "Position sensorless permanent magnet synchronous machine drives—A review," *IEEE Trans. Ind. Electron.*, vol. 67, no. 7, pp. 5830–5842, Jul. 2020.

[17] Y. Lee and J. Ha, "Control method for mono inverter dual parallel surface-mounted permanent-magnet synchronous machine drive system," *IEEE Trans. Ind. Electron.*, vol. 62, no. 10, pp. 6096–6107, Oct. 2015.
[18] D. Luenberger, "Observers for multivariable systems," *IEEE Trans. Autom. Control*, vol. 11, no. 2, pp. 190–197, Apr. 1966.
[19] G. Hostetter and J. Meditch, "Observing systems with unmmeasurable inputs," *IEEE Trans. Autom. Control*, vol. 18, no. 3, pp. 307–308, Jun. 1973.
[20] S.-H. Wang, E. Wang, and P. Dorato, "Observing the states of systems with unmeasurable disturbances," *IEEE Trans. Autom. Control*, vol. 20, no. 5, pp. 716–717, Oct. 1975.
[21] F. Yang and R. W. Wilde, "Observers for linear systems with unknown inputs," *IEEE Trans. Autom. Control*, vol. 33, no. 7, pp. 677–681, Jul. 1988.
[22] M. Darouach, M. Zasadzinski, and S. J. Xu, "Full-order observers for linear systems with unknown inputs," *IEEE Trans. Autom. Control*, vol. 39, no. 3, pp. 606–609, Mar. 1994.
[23] C. Edwards, S. K. Spurgeon, and R. J. Patton, "Sliding mode observers for fault detection and isolation," *Automatica*, vol. 36, no. 4, pp. 541–553, Apr. 2000.
[24] A. Chakrabarty, E. Fridman, S. H. Zak, and G. T.Buzzard, "State and unknown input observers for nonlinear systems with delayed measurements," *Automatica*, vol. 95, pp. 246–253, Sep. 2018.
[25] H. Trinh, T. D. Tran, and T. Fernando, "Disturbance decoupled observers for systems with unknown inputs," *IEEE Trans. Autom. Control*, vol. 53, no. 10, pp. 2397–2402, Nov. 2008.
[26] K. Kalsi, J. Lian, S. Hui, and S. H. Zak, "Brief paper: Sliding mode observers for systems with unknown inputs: A high gain approach," *Automatica*, vol. 46, no. 2, pp. 347–353, Feb. 2010.
[27] F. Zhu, "State estimation and unknown input reconstruction via both reduced-order and high-order sliding mode observers," *J. Process Control*, vol. 22, no. 1, pp. 296–302, Jan. 2012.
[28] Y. Hou, F. Zhu, X. Zhao, and S. Guo, "Observer design and unknown input reconstruction for a class of switched descriptor systems," *IEEE Trans. Syst., Man, Cybern.*, vol. 48, no. 8, pp. 1411–1419, Apr. 2018.
[29] J. Zhang, X. Zhao, F. Zhu, and H. R. Karimi, "Reduced order observer design for switched descriptor systems with unknown inputs," *IEEE Trans. Autom. Control*, vol. 65, no. 1, pp. 287–294, Apr. 2020.
[30] J. Lan, "Asymptotic estimation of state and faults for linear systems with unknown perturbations," *Automatica*, vol. 118, Aug. 2020, Art. no. 108955.
[31] G. Conte, A. M. Perdon, and E. Zattoni, "A structural approach to unknown inputs observation for switching linear systems," *Automatica*, vol. 129, Jul. 2021, Art. no. 109572.
[32] I. Sakhraoui, B. Trajin, and F. Rotella, "Design procedure for linear unknown input functional observers," *IEEE Trans. Autom. Control*, vol. 65, no. 2, pp. 831–838, Feb. 2020.
[33] J. Dávila, M. Tranninger, and L. Fridman, "Finite-time State observer for a class of linear time-varying systems with unknown inputs," *IEEE Trans. Autom. Control*, vol. 67, no. 6, pp. 3149–3156, Jun. 2022.
[34] B. Alenezi, M. Zhang, S. Hui, and S. H. Zak, "Simultaneous estimation of the State, unknown input, and output disturbance in discrete-time linear systems," *IEEE Trans. Autom. Control*, vol. 66, no. 12, pp. 6115–6122, Dec. 2021.
[35] M. Zhang, B. Alenezi, S. Hui, and S. H. Zak, "Unknown input observers for discretized systems with application to networked systems corrupted by sparse malicious packet drops," *IEEE Control Syst. Lett.*, vol. 5, no. 4, pp. 1261–1266, Oct. 2021.
[36] M. Corless and J. Tu, "State and input estimation for a class of uncertain systems," *Automatica*, vol. 34, no. 6, pp. 757–764, Jun. 1998.
[37] F. Mazenc and O. Bernard, "Interval observers for linear time-invariant systems with disturbances," *Automatica*, vol. 47, no. 1, pp. 140–147, Jan. 2011.
[38] F. Zhu, Y. Fu, and T. N. Dinh, "Asymptotic convergence unknown input observer design via interval observer," *Automatica*, vol. 147, Jan. 2023, Art. no. 110744.
[39] G. Liu, H. Zhang, and X. Song, "Position-estimation deviation-suppression technology of PMSM combining phase self-compensation SMO and feedforward PLL," *IEEE J. Emerg. Sel. Topics Power Electron.*, vol. 9, no. 1, pp. 335–344, Feb. 2021.

Tianyi Liu was born in Shanghai, China, in 1989. He received the B.S. degree in information technology engineering from the Tongji University of Information Technology Engineering, Shanghai, China, in 2011, the M.S.E. degree in automation engineering from the Politecnico di Milano of Automation Engineering, Milan, Italy, in 2014, and the Ph.D. degree in electrical engineering from Laboratory LAPLACE, Toulouse University, Toulouse, France, in 2018.

Since 2018, he has been working with Tongji University, Shanghai, China, as an Assistant Professor. His research interests include electric machines, advanced control theory, and aviation applications.

Zhiming Liu was born in Yangzhou, Jiangsu, China, in 1996. He received the B.S. degree in mechanical engineering from the Nantong University of Mechanical Engineering, Nantong, China, in 2018. He has been working toward the M.S.E. degree from the Tongji University of Electronics and Information Engineering, Shanghai, China, since 2019.

His research interests include electric machines, advanced control theory, and artificial intelligence.

Fanglai Zhu received the Ph.D. degree in control theory and control engineering from Shanghai Jiao Tong University, Shanghai, China, in 2001.

Supported by the Chinese government, he worked with Purdue University, West Lafayette, IN, USA, as a Visiting Scholar for six months int the year 2015. Before the year 2007, he was with Guilin University of Electronic Technology (GLIET), Guilin, China, as an Associate Professor for three years and a Professor for two years, respectively. There, he was honored by the Guangxi local government as one of the 100 Young and Middleaged Disciplinary Leaders in Guangxi Higher Education Institutions. Because of the excellent research work he has done in GLIET, he was accepted to join Tongji University, Shanghai, China, in July 2007, as a Professor. His research interests include distributed observer design, model-based fault diagnosis, fault-tolerate control, and security control of multiple agent system consensus.

Dr. Zhu is the member of Professional Committee of Fault Diagnosis and Safety under Chinese Association of Automation. He was the recipient of the third prize of Natural Science Award of Shanghai Science and Technology in 2011. He is also the Editor of *Sensors* and *Insight Automatic Control*.

Zhiyang Mao was born in Zhenjiang, Jiangsu, China, in 2002. He has been working toward the B.S. degree from Tongji University of Civil Engineering, Shanghai, China, since 2020.

His research interests include mechanics, artificial intelligence, and tunnel engineering.